Journal of the European Ceramic Society 23 (2003) 951–959

www.elsevier.com/locate/jeurceramsoc

Effect of grain boundary microcracking on the light transmittance of sintered transparent $MgAl_2O_4$

A.F. Dericioglu, Y. Kagawa*

Institute of Industrial Science, The University of Tokyo 4-6-1, Komaba, Meguro-ku, Tokyo 153, Japan

Received 1 March 2002; accepted 16 June 2002

Abstract

Optically transparent polycrystalline magnesium aluminate spinel ($MgAl_2O_4$) has been fabricated by hot-pressing followed by hot isostatic pressing (HIPing). The effect of microstructure on the light transmittance of the sintered $MgAl_2O_4$ is discussed. The sintered $MgAl_2O_4$ with a thickness of 2 mm has a maximum light transmittance of ~60 and ~70% in the UV–visible and near-IR wavelength regions, respectively, although it contains microcracking along its grain boundaries. Light transmittance losses in the sintered $MgAl_2O_4$ are explained in terms of light scattering at these microcracked grain boundaries: the light transmittance was determined to decrease with increase in the microcracked grain boundary surface area due to pronounced scattering. The light transmittance is well correlated with microcracked grain boundary surface area per unit volume.

Keywords: $MgAl_2O_4$; Microcracking; Microstructure-final; Optical properties; Sintering

1. Introduction

Various kinds of light transmitting ceramics, such as alumina,[1–3] magnesia,[4,5] PLZT,[6,7] thoria-yttria,[8] YAG,[9] $LiAl_5O_8$[10] and magnesium aluminate spinel ($MgAl_2O_4$)[11–18] have been developed and are applied in various engineering fields. Among them, $MgAl_2O_4$ has received considerable attention and has been widely studied[11–18] because of its isotropic optical properties due to the spinel structure and good mechanical properties at high temperatures together with chemical inertness to strong acids and alkali solutions.[19–25]

To use $MgAl_2O_4$ as an optical window material, its microstructure should be optimized since light transmittance is sensitive to microstructures, such as grain boundaries, second phases, impurities and internal flaws, etc. Several reports, although none on $MgAl_2O_4$, have shown the effect of such features on the light transmission properties of various polycrystalline materials.[26–30] The effect of such factors on the light transmittance of $MgAl_2O_4$, however, has not been well studied.

The authors' preliminary study showed that grain boundary microcracking is present in $MgAl_2O_4$ ceramics fabricated by a hot-pressing/hot isostatic pressing process using commercially available MgO and Al_2O_3 powders as starting materials, although it is not expected because of its spinel crystal structure with highly isotropic properties. It is clear that the above mentioned microstructural features are strong sources of the reduction of light transmittance of $MgAl_2O_4$. However, the effect of microcracking on its light transmittance is still an unsolved problem. The present paper has focused on examining the light transmittance of the sintered $MgAl_2O_4$. The effect of microcracking on this transmittance is discussed in terms of light scattering at the microcracked grain boundaries.

2. Experimental procedure

2.1. Preparation of transparent $MgAl_2O_4$

In the present study, $MgAl_2O_4$ ($MgO–Al_2O_3$ molar ratio = 1:1) was obtained by the reaction between MgO

* Corresponding author. Tel.: +81-3-5452-6327; fax: +81-3-5452-6329.

E-mail address: kagawa@iis.u-tokyo.ac.jp (Y. Kagawa).

0955-2219/03/$ - see front matter © 2002 Elsevier Science Ltd. All rights reserved.
PII: S0955-2219(02)00205-4

and Al_2O_3 during the sintering process. A MgO–Al_2O_3 powder mixture was prepared from commercially available, high purity MgO (purity 99.98 wt.%, Type 1000A, Ube Chemicals Co., Ltd., Ube, Japan) and Al_2O_3 (purity 99.99 wt.%, Type TM-DAR, Taimei Chemicals Co., Ltd., Nagano, Japan) powders having average particle sizes less than 0.12 and 0.15 μm, respectively. The powders were mechanically mixed in a MgO–Al_2O_3 molar ratio of 1:1. Mixing was done by wet ball-milling of the starting powders in ethyl alcohol for 24 h, drying the mixture in an evaporator at 80 °C for 5 h and sieving the resulting agglomerates below 500 m particle size.

A bulk $MgAl_2O_4$ was obtained from the mechanically prepared powder through a two-stage operation of hot-pressing followed by hot isostatic pressing (HIPing). Hot-pressing of the compacts was performed at three different temperatures of 1400, 1450 and 1500 °C in vacuum of 10^{-2} Pa for 1 h under a pressure of 50 MPa. A square shaped graphite hot-pressing die with an inner lateral size of 65 mm was used, and hot-pressed compacts with a thickness of ~6 mm were obtained.

Hot-pressed material was hot-isostatically pressed (HIPed) in order to obtain the maximum possible densification, which is a key to achieving high light transmittance. HIP of the material was performed in argon at 1900 °C for 1 h under a pressure of 189 MPa. Hot-pressed $MgAl_2O_4$ was directly HIPed in a pressure vessel without a coupsol. Thereafter, as sintered $MgAl_2O_4$ compacts were mechanically cut to ~2 and ~4 mm thick blocks, and their surfaces were polished by a standard metallurgical process. Final polishing of the blocks was done using a 0.5 μm diamond paste finish to obtain a flat and parallel surface for further light transmittance measurements. Fig. 1 shows the definition of *x–y–z* coordinates of the sintered $MgAl_2O_4$ specimens with hot-pressing direction.

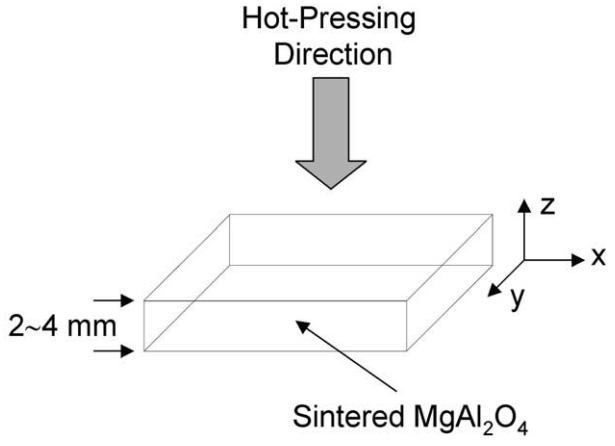

Fig. 1. Definition of *x–y–z* coordinates of the tested samples with hot-pressing direction.

2.2. Characterization

2.2.1. Observation of microstructure

The microstructure of the sintered $MgAl_2O_4$ was observed using a conventional optical microscope (BUH, Olympus Co., Ltd., Tokyo, Japan) under reflective light and cross-polarized transmission light. The polished specimens were thermal-etched in ambient air at 1200 °C for 1 h. Etched surfaces perpendicular to the hot-pressing direction (*x–y* plane: Fig. 1) were observed. The average grain size of each sample was determined using a quantitative metallographic technique,[31] intersection method. Additionally, densities of the samples were measured using Archimedes' principle, at room temperature (26 °C) with ethyl alcohol as the immersion medium. The accuracy of the density measurement was $\sim \pm 0.003$ g/cm^3.

2.2.2. Crystalline structure

X-ray diffraction analysis was performed using an X-ray diffractometer (RINT2500, Rigaku Corporation, Tokyo) with a Mo target to identify the crystalline structure of the sintered $MgAl_2O_4$. The analysis was done on the polished surfaces of the bulk samples (*x–y* plane) that were perpendicular to the hot-pressing direction.

2.2.3. Chemical composition

A small amount of $MgAl_2O_4$ powder (~0.1 g), which was crushed (in a silica mortar) from the sintered $MgAl_2O_4$ compacts, was mixed with potassium carbonate and boric acid, and this mixture was melted in a high purity Pt crucible. The molten mixture was dissolved in nitric and hydrochloric acids, and the solution was diluted with deionized water to a total amount of 100 ml. Chemical composition of the diluted solution was determined by an inductively coupled plasma spectrometer (SPS 4000 Plasma Spectrometer, Seiko Instrument Inc., Tokyo).

2.2.4. Light transmittance of sintered $MgAl_2O_4$

In-line light transmittance of the sintered $MgAl_2O_4$ parallel to the hot-pressing direction (*z*-direction) was measured using samples with a thickness of 2.0 ± 0.02 mm. UV–visible wavelength range ($\lambda = 200$–1100 nm) transmittance measurements were made by a transmission optical spectrometer (V-530 type, Jasco Corp., Tokyo) at room temperature (24 °C) in air. The resolution of the spectrometer in the measured wavelength range was less than 2 nm. For each sample, four different transmission spectra were obtained by rotating them by 90° at each measurement to eliminate polarization effects, and the average value of these measurements was used for the analyses. Near-IR transmittance of the sintered $MgAl_2O_4$ ($\lambda = 2.5$–25 μm) was also measured with a Fourier transformation infrared ray analyzer

(FTIR-4200, Shimadzu Corp., Kyoto, Japan) under the same conditions and the measurement procedure of the UV–visible wavelength range measurement.

2.2.5. Light scattering behavior

To observe light scattering behavior of the sintered $MgAl_2O_4$, it was irradiated by a 4-mW non-polarized He–Ne laser beam in the x-direction through the polished side surface of each sample, and images were photographed from the z-direction through the polished upper surfaces of the samples using an optical microscope. Additionally, angular scattering profile of the sintered $MgAl_2O_4$ was determined using a home-made light scattering measurement optical system (Fig. 2). The sample surface was irradiated by a 4-mW He–Ne laser ($\lambda = 632.8$ nm), and scattering behavior of the beam was observed by a high sensitive CCD detector (576-G/1, Princeton Instruments, USA) coupled with a spectrometer (resolution: 0.8 nm, SpectraPro 275, Acton, USA). Diameter of the incident light at the specimen surface was $\sim$0.5 mm. Detection of the scattered light was done by an optical fiber with an effective detection area diameter of 1 mm at its tip. During detection, shutter speed of the CCD detector was controlled up to nanosecond order to allow accurate measurements at scattering angles close to the incident beam. Here, the direction of the incident laser beam is defined as $\theta = 0^\circ$ [Fig. 2(b)]. The tip of the optical fiber was placed 150 mm away from the exit plane of the beam (i.e. exit surface of the specimen). Data collection was done at every 2° at the weak scattering portion of the profile; however, at angles close to 0° (incident beam) the data was collected at every 0.5° to achieve higher accuracy.

3. Experimental results

3.1. Microstructure and chemical composition

Fig. 3 shows the microstructure of sintered $MgAl_2O_4$ taken from their surfaces perpendicular to the hot-pressing direction together with their hot-pressing temperature, T, and average grain size, $\overline{d}$. The average grain size (mean intercept length) changed with the sintering condition, and the smallest value was observed on the specimen hot-pressed at 1450 °C. The distribution of the grain size also depends on the sintering condition, and the grain size of the specimen hot-pressed at 1450 °C was determined to be within the narrowest range (Table 1).

Microstructural examination of the sintered $MgAl_2O_4$ under the cross-polarized transmission light revealed the existence of microcracking along the grain boundaries. The micrograph shown in Fig. 4 demonstrates that the microcracks are located along the grain boundaries as indicated by arrows. The microcrack density of the sintered $MgAl_2O_4$ was evaluated from the micrographs

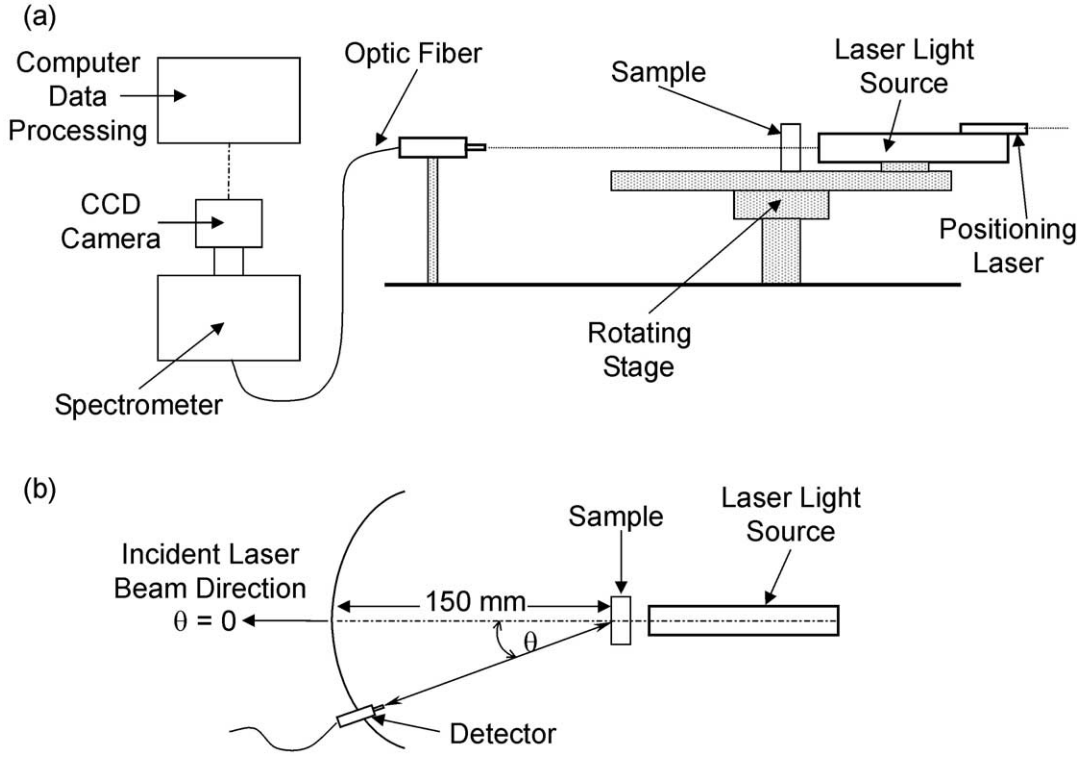

Fig. 2. (a) Schematic drawing of the home-made optical system to measure the scattered light intensity distribution, (b) definition of scattering angle, θ.

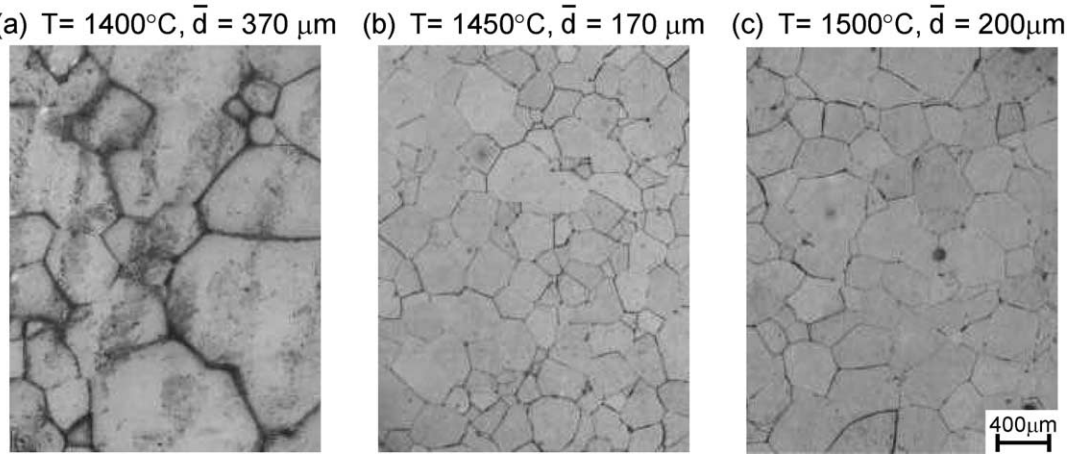

Fig. 3. Microstructure of sintered $MgAl_2O_4$ ceramics with their hot-pressing temperature, T, average grain size, $\bar{d}$.

Table 1
Microstructural parameters, relative density and the chemical composition of the sintered $MgAl_2O_4$ ceramics

Hot-pressing temperature (°C)	Grain size distribution range (μm)	Microcracked grain boundary surface area per unit volume S_v^{Mc} (mm^{-1})	Relative theoretical density (%)	Chemical composition (wt.%)		
				Al	Mg	Fe
1400	100–1200	0.29	99.88	37.15	15.05	0.05
1450	50–450	0.54	99.96	40.94	14.75	0.05
1500	50–550	0.78	99.93	39.18	14.33	0.03
		Stoichiometric Al (wt.%)		37.93		
		Stoichiometric Mg (wt.%)			17.09	

using a stereological relationship,[31] assuming that the microcracks are located randomly in the specimen. The amount of microcracking (microcracked grain boundary surface area per unit volume), S_v^{Mc}, is defined as,

$$S_v^{Mc} = 2P_L^{Mc} \quad (1)$$

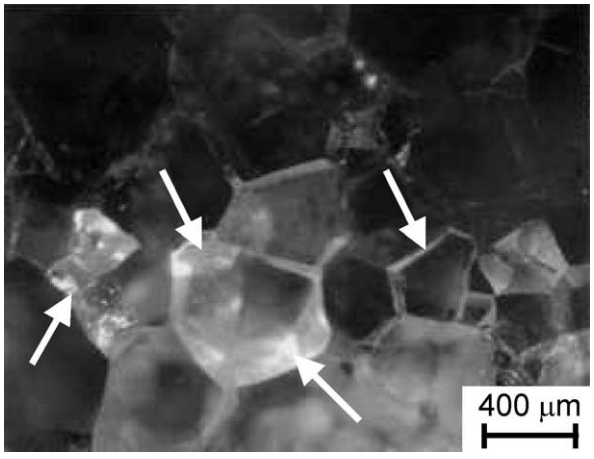

Fig. 4. Micrograph of the polished section of sample hot-pressed at 1400 °C under cross-polarized transmission light, showing microcracking along grain boundaries (arrows indicate example of microcracked grain boundaries).

where P_L^{Mc} is the density of the intersection points of the microcracked grain boundaries with the test lines piercing the surface of the specimen. Here, a regular system of test lines was used, whose total length was chosen arbitrarily as 25 mm on the polished specimen surface at a magnification of $\sim\times40$. The obtained values of S_v^{Mc} are listed in Table 1 for all of the samples. It is known that inhomogeneous size distribution and packing of the powders lead to non-uniform sintering rates causing internal residual stresses and stress gradients to develop in the structure, resulting in microcracking. In this study, details of the reason for the microcracking behavior are unclear, however, it is probable that non-uniform grain size distribution in the microstructure of the sintered $MgAl_2O_4$ is a strong source of grain boundary microcracking. In several studies microcracking at the grain boundaries of ceramics with cubic structure was reported,[32] although it is not usually encountered in cubic crystals like spinel because of their highly isotropic nature.

The relative density, chemical composition and impurity content of the sintered $MgAl_2O_4$ are also listed in Table 1. The measured densities are changing between 99.88 and 99.96% of the theoretical density of $MgAl_2O_4$ ($\rho_{theo} = 3.58$ g/cm^3, for the hot-pressed $MgAl_2O_4$),[12] which is within the accuracy range of the measurement. Chemical composition of the sintered

$MgAl_2O_4$ shows a slight shift from the stoichiometry of the magnesium aluminate spinel since the measured Mg and Al percentages differ from the stoichiometric values of 17.09 and 37.93 wt.% calculated from their mass ratios in $MgAl_2O_4$, respectively. This might have been caused by the inhomogeneous distribution of the starting MgO and Al_2O_3 powders during the mechanical mixing. Additionally, a small amount of Fe, ~0.05%, was detected as an impurity in the sintered $MgAl_2O_4$, which could have been introduced into the raw materials during the mechanical powder preparation stage.

Fig. 5 shows a typical XRD profile of the sintered $MgAl_2O_4$ hot-pressed at 1400 °C [Fig. 5(b)] as a representative together with the standard pattern[33] of the synthetic stoichiometric $MgAl_2O_4$ [Fig. 5(a)]. With this result presence of $MgAl_2O_4$ as a single phase in the fabricated ceramics is evidenced. However, the slight shift in the positions of the detected peaks compared to the standard pattern is caused by the nonstoichiometry of the composition, and the difference in their intensities is caused by the large average grain size; these might be the consequences of the used powder preparation technique and the inhomogeneous grain size distribution, respectively.

3.2. Appearance and light transmittance of sintered $MgAl_2O_4$

Typical appearances of the sintered $MgAl_2O_4$ (thickness = 4.0 ± 0.02 mm) with their hot-pressing temperatures are shown in Fig. 6. The underlying letters are legible through all of the samples, suggesting good light transmittance of the $MgAl_2O_4$ at the visible wavelength region. The sintered $MgAl_2O_4$ hot-pressed at 1400 °C [Fig. 6(a)] has the most clear optical transparency of all the fabricated samples.

Light transmittance of the sintered $MgAl_2O_4$ in the UV–visible wavelength range measured through 2-mm thick blocks parallel to the hot-pressing direction is shown in Fig. 7. The transmittance spectra of the samples show good correlation with their appearance. The clear transparent sample hot-pressed at 1400 °C has the maximum transmittance of ~60% above the wavelength of 700 nm. However, its transmittance decreases to ~30–60% in the visible wavelength range. The other two samples that are slightly darker in color have lower transmittance values of ~15–30% at a wavelength range from 300 to 1100 nm. Near-IR wavelength range transmittance values of the sintered $MgAl_2O_4$ are higher than that of the UV–visible wavelength range, however, the values follow the same decreasing order with the hot-pressing temperature, as can be seen in Fig. 8. The sintered $MgAl_2O_4$ hot-pressed at 1400 °C has the highest transmittance value of above 70% at a wavelength range from 2.5 to 5 μm. Near-IR wavelength range transmittance of the sintered $MgAl_2O_4$ becomes nearly zero at wavelengths longer than 6.5 μm, which is associated with the lattice vibrations.[34] The peak observed in all of the spectra at ~4.25 μm is caused by the presence of CO_2 in the measurement atmosphere, since the measurements were done in ambient air[35] and continuous changes in the concentration of CO_2 did not allow accurate background corrections.

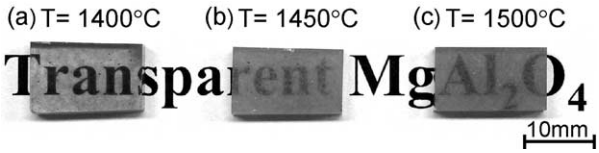

Fig. 6. Appearance of sintered $MgAl_2O_4$ ceramics (thickness: ~4 mm) with their hot-pressing temperature, T: (a) $T = 1400$ °C, (b) $T = 1450$ °C, (c) $T = 1500$ °C.

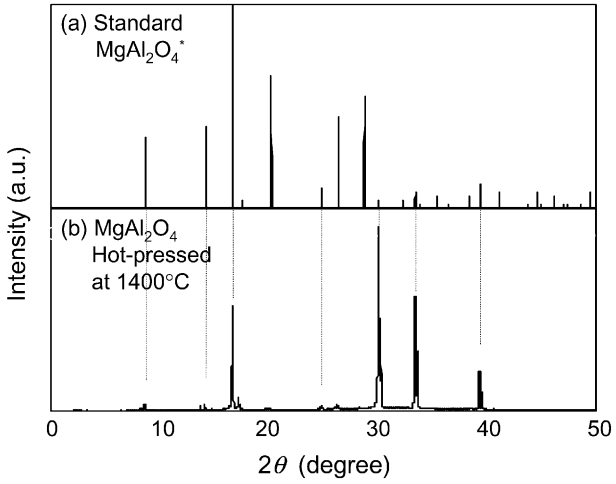

Fig. 5. XRD patterns of (a) standard synthetic spinel and (b) $MgAl_2O_4$ hot-pressed at 1400 °C.

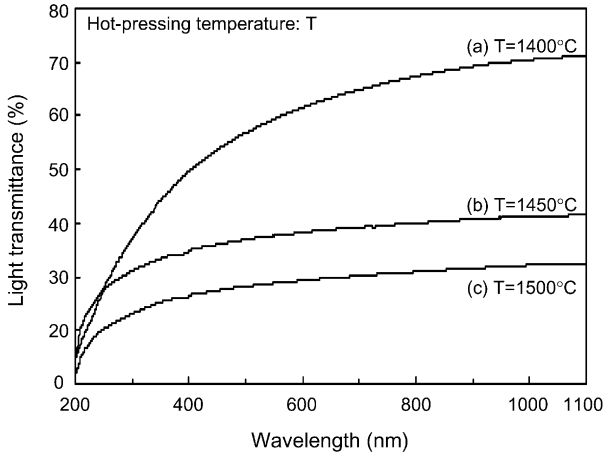

Fig. 7. Light transmittance spectra of the sintered $MgAl_2O_4$ in the UV–visible wavelength range.

3.3. Light scattering behavior

Photographs shown in Fig. 9 demonstrate the spreading behavior of the laser beam in the sintered $MgAl_2O_4$. Some of the grain boundaries are distinguished as bright lines, which is caused by the presence of microcracking at the grain boundaries. The spreading behavior of the laser beam differs in each sample, and the broadening of the beam increases with increasing number of microcracks (S_v^{Mc}).

Fig. 10 shows the angular scattering profiles of the sintered $MgAl_2O_4$ specimens. This figure indicates quantitative understanding of the light scattering behavior, shown in Fig. 9. The specimen with the minimum amount of grain boundary microcracking has a sharp profile with the highest specular transmission. On the other hand, nonforward scattering increases with increase in the number of grain boundary microcracking, and therefore the profiles become broader with decreasing specular transmission component. Although not on $MgAl_2O_4$, a similar behavior was observed between the light scattering behavior and microstructural features of several polycrystalline ceramics.[30]

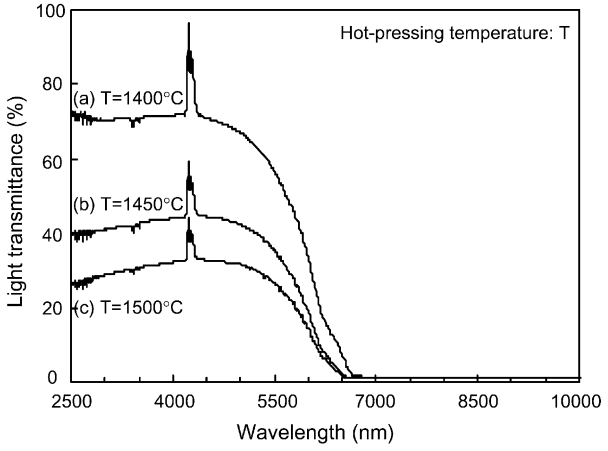

Fig. 8. Light transmittance spectra of the sintered $MgAl_2O_4$ in the near-IR wavelength range.

4. Discussion

It has been known that light transmittance of polycrystalline ceramics is affected by various factors such as porosity, presence and amount of second phases and impurities, grain boundaries and the surface condition of the material under investigation.[34] However, since in the present study the porosity content is considerably low, and $MgAl_2O_4$ is the single phase in the structure, it can be thought that the major source of the light transmittance losses is the microcracking formed at grain boundaries. In doing this, it should be noted that the scattering effect of microcracked regions is much more stronger compared to the effect of the rest of the grain boundaries, and hence the effect of grain boundaries can be neglected. For this reason, hereafter, the relationship between the light transmittance and amount of microcracking of the sintered $MgAl_2O_4$ will be discussed.

Here, it is assumed that maximum light transmittance, T^*, occurs for a single crystal $MgAl_2O_4$ without any scattering sources. The maximum light transmittance in that condition for a given wavelength is given by,

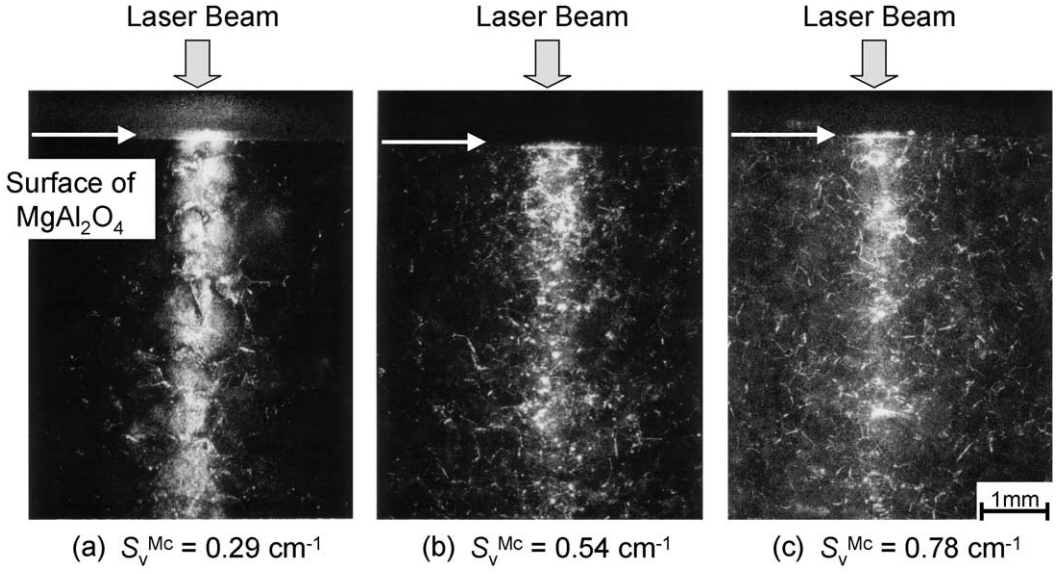

Fig. 9. Scattering behavior of the laser beam in the sintered $MgAl_2O_4$ with different amounts of microcracking, S_v^{Mc} (microcracked grain boundary surface area per unit volume).

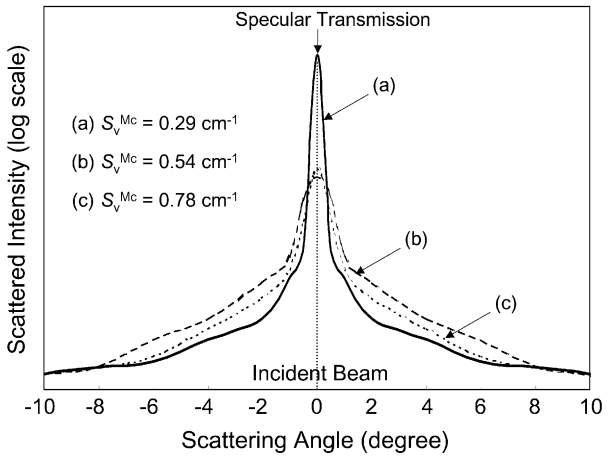

Fig. 10. Angular distribution of the intensity of scattered light transmitting through microcracked $MgAl_2O_4$ with different amounts of microcracking, S_v^{Mc}.

$$T^* = (1-R)^2\exp(-\alpha t) \tag{2}$$

and

$$R \approx \frac{(\bar{n}-n_a)^2}{(\bar{n}+n_a)^2} \tag{3}$$

where α is the loss factor, t is the thickness of the sample, $\bar{n}$ is the mean refractive index of a single crystal $MgAl_2O_4$, and n_a is the refractive index of air ($\approx$1.000). The mean refractive index, $\bar{n}$, of the $MgAl_2O_4$ single crystal at a wavelength λ is obtained from its dispersion function[34] of,

$$n^{-2}-1 = \frac{1.8938\lambda^2}{\lambda^2-0.09942^2} + \frac{3.0755\lambda^2}{\lambda^2-15.826^2}. \tag{4}$$

Calculation at the wavelengths of $\lambda = 1000$, 700 and 500 nm yields mean refractive index values of $\bar{n} = 1.70$, 1.71 and 1.72, respectively. It should be noted that absorption of the single crystal $MgAl_2O_4$ is negligible at the visible wavelength region.[36] Using Eqs. (2) and (3) with the calculated $\bar{n}$ values and $\alpha = 0$, the maximum light transmittance of the single crystal $MgAl_2O_4$ is found to be $T^* \cong 0.87$ for the wavelength range of concern. The estimated value is higher than that of the measured light transmittance of the sintered $MgAl_2O_4$, suggesting light transmission loss by microcracking.

Generally, the loss factor, α, in Eq. (2) is approximated by,

$$\alpha \approx \alpha_{abs} + \alpha_{sca} \tag{5}$$

where α_{abs} is the absorption loss factor and α_{sca} is the loss factor by light scattering. Both of these factors are written as the sum of loss factors resulting from different contributors. In the present case, the scattering loss factor of the microcracked polycrystalline $MgAl_2O_4$ is given as,

$$\alpha_{sca} = \alpha^{Gb} + \alpha^{Mc} \tag{6}$$

where α^{Gb} and α^{Mc} are the scattering loss factors due to the existence of grain boundaries and microcracking, respectively. Since the grain boundary scattering, α^{Gb}, is assumed to be negligible compared to the scattering caused by microcracking ($\alpha^{Gb} << \alpha^{Mc}$), the scattering loss factor reduces to $\alpha_{sca} \approx \alpha^{Mc}$. With the additional assumption that α_{abs} is negligibly small ($\alpha_{abs} \approx 0$) for the measured wavelength range, light transmittance of the sintered $MgAl_2O_4$ is given by,

$$T \approx (1-R)^2\exp(-\alpha^{Mc} t). \tag{7}$$

Fig. 11 shows plots of logarithm of normalized light transmittance (T/T^*), ℓn T/T^*, versus microcracked grain boundary surface area per unit volume, S_v^{Mc}, for three different wavelengths. The plots following a straight line suggest that the light transmittance can be expressed as,

$$T \approx (1-R)^2\exp(-\beta' S_v^{Mc} t) \tag{8}$$

where β' is a constant. The deviation of the data points from the linear behavior can be attributed to the slight absorption of the sintered $MgAl_2O_4$, which was neglected in the present discussion and has a slight effect on the predicted loss factor, α. Nevertheless, agreement of a best fit to the experimental result with Eq. (8) indicates that the major loss in the light transmittance of sintered $MgAl_2O_4$ originates from light scattering at microcracked grain boundaries.

Summarizing the results, light transmittance of the sintered polycrystalline $MgAl_2O_4$ depends on its microstructure, especially on the amount of microcracking.

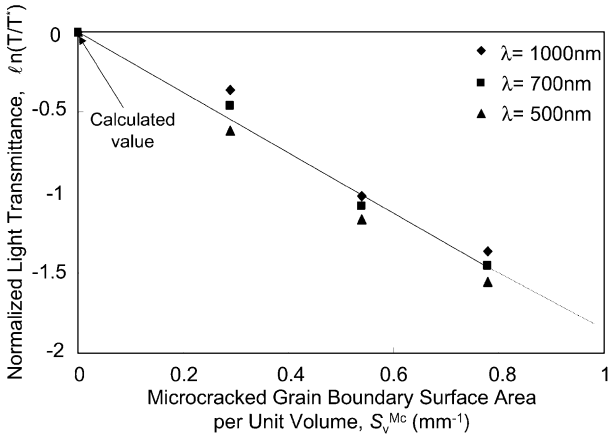

Fig. 11. Natural logarithm of normalized light transmittance (at $\lambda = 500$, 700, 1000 nm) versus microcracked grain boundary surface area per unit volume, S_v^{Mc}, of the sintered $MgAl_2O_4$.

Light transmittance of the sintered $MgAl_2O_4$ is explained by the microcracked grain boundary surface area per unit volume, S_V^{Mc}. It is clear that microcracking should be avoided in the sintered $MgAl_2O_4$ to achieve highest light transmittance. However, further study is needed to explain the origin of grain boundary microcracking behavior of the cubic $MgAl_2O_4$.

5. Conclusions

Optically transparent $MgAl_2O_4$ has been fabricated by hot-pressing followed by HIPing from pure MgO and Al_2O_3 powders. Light transmittance of the sintered $MgAl_2O_4$ was discussed in terms of its microstructure and the following results were obtained:

1. Light transmittance values of the sintered $MgAl_2O_4$ measured in the UV–visible and near-IR wavelength regions revealed that, although there is a change in these values with the hot-pressing temperature, the sample hot-pressed at 1400 °C has the maximum transmittance of over 60 and 70% in the UV–visible and near-IR wavelength regions, respectively, with a high degree of transparency.
2. Microcracking was observed along the grain boundaries of the sintered $MgAl_2O_4$ and was determined to be the major source reducing the light transmittance of $MgAl_2O_4$ by causing extensive scattering. A linear relationship between the natural logarithm of light transmittance and microcracked grain boundary surface area per unit volume was obtained.

References

1. Yamamoto, N. and Mizuno, Y., Translucent alumina. *Am. Ceram. Soc. Bull.*, 1972, **51**, 326.
2. Li, Y., Su, X., Song, L., Zhang, B. and Meng, X., Scattering window material: transparent Al_2O_3 ceramics and its fabrication. *Chin. Phys. Lett.*, 1995, **12**, 393–395.
3. Bennison, S. J. and Harmer, M. P., A history of the role of MgO in the sintering of α-Al_2O_3. *Ceram. Trans.*, 1990, **7**, 13–49.
4. Benecke, M. W., Olson, N. E. and Pask, J. A., Effect of LiF on hot-pressing of MgO. *J. Am. Ceram. Soc.*, 1967, **50**, 365–368.
5. Rice, R. W., Hot-pressing of MgO with NaF. *J. Am. Ceram. Soc.*, 1971, **54**, 205–207.
6. Yoshikawa, Y. and Tsuzuki, K., Fabrication of transparent lead lanthanum zirconate titanate ceramics from fine powders by two-stage sintering. *J. Am. Ceram. Soc.*, 1992, **75**, 2520–2528.
7. Haertling, G. H. and Land, C. E., Hot-pressed (Pb, La) (Zr, Ti)O_3 ferroelectric ceramics for electrooptic applications. *J. Am. Ceram. Soc.*, 1971, **54**, 1–10.
8. Hartmanova, M., Hanic, F., Pisarcik, M. and Ullmann, H., Microstructure and physical properties of transparent throria-yttria ceramics. *J. Mat. Sci.*, 1991, **26**, 4313–4316.
9. Ikesue, A., Furusato, I. and Kamata, K., Fabrication of polycrystalline, transparent YAG ceramics by a solid-state reaction method. *J. Am. Ceram. Soc.*, 1995, **78**, 225–228.
10. Gazza, G. E., Hot-pressing of $LiAl_5O_8$. *J. Am. Ceram. Soc.*, 1972, **55**, 172–173.
11. Bratton, R. J., Translucent sintered $MgAl_2O_4$. *J. Am. Ceram. Soc.*, 1974, **57**, 283–286.
12. Roy, D. W., Hot-pressed $MgAl_2O_4$ for ultraviolet (UV), visible, and infrared (IR) optical requirements. *Proc. SPIE*, 1981, **297**, 3–18.
13. Wang, C-T., Lin, L-S. and Yang, S-J., Preparation of $MgAl_2O_4$ spinel powders via freeze-drying of alkoxide precursors. *J. Am. Ceram. Soc.*, 1992, **75**, 2240–2243.
14. Tsai, D. S., Wang, C. T., Yang, S. J. and Hsu, S. E., Hot isostatic pressing of $MgAl_2O_4$ spinel infrared windows. *Mat. Manufact. Processes*, 1994, **9**, 709–719.
15. Shimada, M., Endo, T., Saito, T. and Sato, T., Fabrication of transparent spinel polycrystalline materials. *Mat. Lett.*, 1996, **28**, 413–415.
16. Ting, C-J. and Lu, H-Y., Hot-pressing of magnesium aluminate spinel—I: kinetics and densification mechanism. *Acta Mater.*, 1999, **47**, 817–830.
17. Ting, C-J. and Lu, H-Y., Hot-pressing of magnesium aluminate spinel—II: microstructure development. *Acta Mater.*, 1999, **47**, 831–840.
18. Gilde, G., Patel, P. and Patterson, M., A Comparison of hot-pressing, rate-controlled sintering, and microwave sintering of magnesium aluminate spinel for optical applications. *Proc. SPIE*, 1999, **3705**, 94–104.
19. Green, K. E., Hastert, J. L. and Roy, D. W., Polycrystalline $MgAl_2O_4$ spinel a broad band optical material for offensive environments. *Proc. SPIE*, 1989, **1112**, 2–8.
20. Roy, D. W. and Martin, G. G. Jr., Advances in spinel optical quality, size/shape capability and applications. *Proc. SPIE*, 1992, **1760**, 2–13.
21. Swab, J. J., LaSalvia, J. C., Gilde, G. A., Patel, P. J. and Motyka, M. J., Transparent armor ceramics: AlON and spinel. *Ceram. Eng. Sci. Proc.*, 1999, **20**, 79–84.
22. Patterson, M. C. L., Caiazza, J. E. and Roy, D. W., Transparent spinel development. *Proc. SPIE*, 2000, **4102**, 59–68.
23. Patterson, M. C. L., Caiazza, J. E., Gilde, G. and Roy, D. W., Transparent $MgAl_2O_4$ spinel. *Ceram. Eng. Sci. Proc.*, 2000, **21**, 423–430.
24. Roy, D. W. and Hastert, J. L., Polycrystalline $MgAl_2O_4$ spinel for high temperature windows. *Ceram. Eng. Sci. Proc.*, 1983, **4**, 502–509.
25. Hing, P., Fabrication of translucent magnesium aluminate spinel and its compatibility in sodium vapour. *J. Mater. Sci.*, 1976, **11**, 1919–1926.
26. Grimm, N., Scott, G. E. and Sibold, J. D., Infrared transmission properties of high density alumina. *Ceram. Bull.*, 1971, **50**, 962–965.
27. Peelen, J. G. J. and Metselaar, R., Light scattering by pores in polycrystalline materials: Transmission properties of alumina. *J. Appl. Phys.*, 1974, **45**, 216–220.
28. Erneta, M. and Stockler, H. A., Light scattering by pores in ceramic (Pb, La) (Zr, Ti) O_3. *J. Am. Ceram. Soc.*, 1973, **56**, 394–395.
29. Hanna, R., Infrared properties of magnesium oxide. *J. Am. Ceram. Soc.*, 1965, **48**, 376–380.
30. Schroeder, J. and Rosolowski, J. H., Light scattering in polycrystalline materials. *Proc. SPIE*, 1981, **297**, 156–168.
31. Kurzydlowski, K. J. and Ralph, B., *The Quantitative Description of the Microstructure of Materials*. CRC Press, Boca Raton, FL, 1995.
32. Ahlborn, K., Kagawa, Y. and Okura, A., The influence of the network of microcracks upon the crack propagation behavior

inside of transparent zirconia. *Fracture Mech. Ceram.*, 1992, **10**, 47–58.
33. Anon., *National Bureau Standards (US)* Monogr. 25, 9 25, 1971.
34. Baas, M., ed., *Handbook of Optics*. McGraw-Hill, New York, 1995.
35. Wolfe, W. L. and Zissis, G. J., *The Infrared Handbook*. ONR, Department of Navy, Washington, DC, 1978.
36. White, G. S., Jones, R. V. and Crawford, J. H. Jr., Optical spectra of $MgAl_2O_4$ crystals exposed to ionizing radiation. *J. Appl. Phys.*, 1982, **53**, 265–270.